MECHANISMS OF HYDROGEN-ASSISTED FRACTURE IN AUSTENITIC STAINLESS STEEL WELDS

B.P. Somerday[1], D.K. Balch[1], P. Novak[2], and P. Sofronis[2]
[1]Sandia National Laboratories, Livermore, CA 94550 USA
[2]Department of Theoretical and Applied Mechanics, University of Illinois, Urbana, IL 61801 USA

ABSTRACT

The objective of this study was to quantify the hydrogen-assisted fracture susceptibility of gas-tungsten arc (GTA) welds in the nitrogen-strengthened, austenitic stainless steels 21Cr-6Ni-9Mn (21-6-9) and 22Cr-13Ni-5Mn (22-13-5). In addition, mechanisms of hydrogen-assisted fracture in the welds were identified using electron microscopy and finite-element modeling. Elastic-plastic fracture mechanics experiments were conducted on hydrogen-charged GTA welds at 25°C. Results showed that hydrogen dramatically lowered the fracture toughness from 412 kJ/m^2 to 57 kJ/m^2 in 21-6-9 welds and from 91 kJ/m^2 to 26 kJ/m^2 in 22-13-5 welds. Microscopy results suggested that hydrogen served two roles in the fracture of welds: it promoted the nucleation of microcracks along the dendritic structure and accelerated the link-up of microcracks by facilitating localized deformation. A continuum finite-element model was formulated to test the notion that hydrogen could facilitate localized deformation in the ligament between microcracks. On the assumption that hydrogen decreased local flow stress in accordance with the hydrogen-enhanced dislocation mobility argument, the finite-element results showed that deformation was localized in a narrow band between two parallel, overlapping microcracks. In contrast, in the absence of hydrogen, the finite-element results showed that deformation between microcracks was more uniformly distributed.

1 INTRODUCTION

Austenitic stainless steels are well suited for structural applications in hydrogen-containing environments, since these alloys are highly resistant to hydrogen-assisted fracture (Caskey [1]). Although hydrogen-assisted fracture of austenitic steels has been extensively studied, few efforts have focused on welds. Fusion welds in austenitic steels are generally designed to solidify as primary ferrite, which results in retention of a small amount of δ-ferrite following the solid-state transformations that occur during cooling. Hydrogen-assisted fracture in the weld fusion zone could be more severe compared to that in the base metal due to the presence of retained δ-ferrite (Brooks [2]).

The objective of this study was to quantify the hydrogen-assisted fracture susceptibility of gas-tungsten arc (GTA) welds in the nitrogen-strengthened, austenitic stainless steels 21Cr-6Ni-9Mn (21-6-9) and 22Cr-13Ni-5Mn (22-13-5) using fracture mechanics methods. In addition, mechanisms of hydrogen-assisted fracture in the welds were identified using electron microscopy of fracture surfaces and sub-surface regions. A physical model for hydrogen-assisted fracture in the welds was formulated from microscopy evidence. Elements of the physical model were tested using a finite-element model, which included effects of hydrogen on deformation.

2 EXPERIMENTAL PROCEDURES

The 21-6-9 (composition 19.27Cr-6.98Ni-9.68Mn-0.28N in wt%) and 22-13-5 (composition 20.86Cr-12.05Ni-4.99Mn-0.37N in wt%) base metals were procured as forgings having 75 mm square cross sections. The 0.2%-offset yield strengths of the 21-6-9 and 22-13-5 base metals were measured as 485 MPa and 476 MPa, respectively. A U-groove approximately 25 mm deep x 20 mm wide (maximum width) was machined along the length of each square bar. Each groove was

subsequently filled with matched filler wire using approximately 30 GTA weld passes. Maximum interpass temperatures of 500°C were maintained during welding.

The design and testing of compact tension (CT) specimens were accomplished in accordance with ASTM standard E1737-96 ([3]). The CT specimens from 21-6-9 had a width of 26.5 mm, a gross thickness of 6.0 mm, and a net thickness of 4.6 mm between the sidegrooves. The in-plane and thickness dimensions of the 22-13-5 specimens were two times the size of the 21-6-9 specimens (Balch [4]). The CT specimens were fatigue precracked in air to final crack length-to-width ratios from 0.48 to 0.63 under a final maximum stress-intensity factor (K_{MAX}) of about 34 MPa√m. The CT specimens were machined from the bars so that fatigue precracks terminated in the weld fusion zone near the base of the U-groove (Balch [4]). The fatigue-precracked specimens were thermally charged with hydrogen in either 138 MPa gas at 300°C for 29 days (21-6-9 specimens) or in 69 MPa gas at 300°C for 138 days (22-13-5 specimens). These charging schedules produced measured total hydrogen concentrations of 230 wppm and 120 wppm, respectively, for 21-6-9 and 22-13-5. Fracture mechanics tests were conducted in air at a constant actuator displacement rate of 0.4 mm/min. Crack propagation was monitored using the direct-current potential difference (DCPD) technique. The time to reach fracture initiation was about 2 min for each hydrogen-charged specimen.

Characterization of weld microstructures, fracture surfaces, and sub-surface fracture profiles was accomplished by a combination of optical and scanning electron microscopy (SEM) as well as x-ray diffraction.

3 RESULTS

The fusion zones of 21-6-9 and 22-13-5 GTA welds contained δ-ferrite along former dendrite cores in an austenite (γ) matrix. Backscattered electron images showing δ-ferrite and γ in 21-6-9 and 22-13-5 fusion zones are in Figure 1. The fatigue precrack terminated in the fusion zone with an orientation parallel to the aligned dendritic solidification structure in the center of the weld. Figure 1(b) also shows the presence of a bright phase in 22-13-5, which was identified as the intermetallic phase σ (nominal composition FeCr) (Balch [4]). The σ phase likely transformed from δ-ferrite due to weld deposit reheating during the multi-pass weld procedure.

Hydrogen dramatically lowered the fracture resistance of both 21-6-9 and 22-13-5 GTA welds. Figure 2 shows J *vs* Δa crack-growth resistance curves for the two different welds in the hydrogen-charged and uncharged conditions. Duplicate results are plotted for each condition in Figure 2, except for the uncharged 22-13-5 weld, where only one experiment was conducted. Hydrogen lowered fracture initiation toughness from 412 kJ/m^2 (J_{IC}) to 57 kJ/m^2 (J_{IH}) in 21-6-9 GTA welds

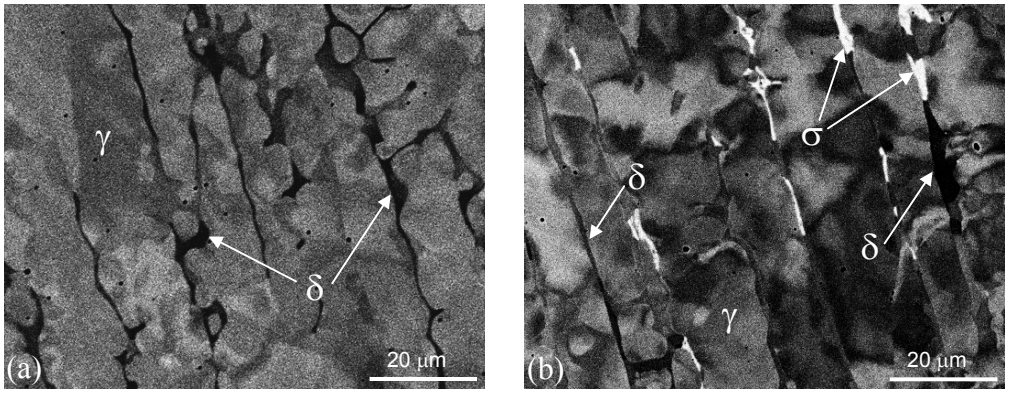

Figure 1: Backscattered electron images of weld fusion zones for (a) 21-6-9 and (b) 22-13-5.

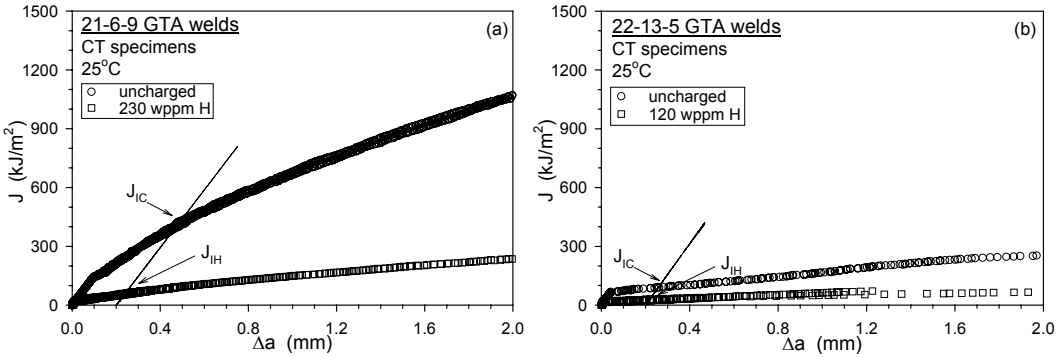

Figure 2: Crack-growth resistance curves for hydrogen-charged and uncharged GTA welds of (a) 21-6-9 and (b) 22-13-5 stainless steels.

and from 91 kJ/m^2 (J_{IC}) to 26 kJ/m^2 (J_{IH}) in 22-13-5 GTA welds. The low J_{IC} value (91 kJ/m^2) for the uncharged 22-13-5 weld was attributed to the presence of low-ductility σ phase (Balch [4]).

Hydrogen altered the fracture modes in 21-6-9 and 22-13-5 GTA welds. Fracture initiation in each uncharged weld involved the nucleation, growth, and coalescence of microvoids. Figure 3 shows secondary electron images of fracture surfaces from the hydrogen-charged 21-6-9 and 22-13-5 welds. In contrast to the uncharged welds, fracture initiation in the hydrogen-charged welds did not involve extensive plasticity, particularly for the 22-13-5 welds. In addition, the fracture surfaces for hydrogen-charged welds reveal features that are oriented parallel to the crack propagation direction. This suggests that fracture was associated with the aligned dendritic structure of the welds. The common feature exhibited by both welds in Figure 3 is marked topography changes, where flat areas at different elevations are separated by steep "walls". (These topography changes are not readily apparent in Figure 3 but were observed using stereo pairs.)

Further insight into the fracture process was gained by observing fracture surface profiles using backscattered electron imaging. Figure 4 shows regions adjacent to the fracture surface for hydrogen-charged 22-13-5 welds. In Figure 4(a) a "stepped" fracture profile is clearly seen. The horizontal sections of the steps are associated with the dendritic structure. Figure 4(b) reveals a possible mechanism for creating the vertical sections of the steps. In Figure 4(b), a box encloses a region where lengths of δ-ferrite have apparently been reoriented by shear. This evidence suggests

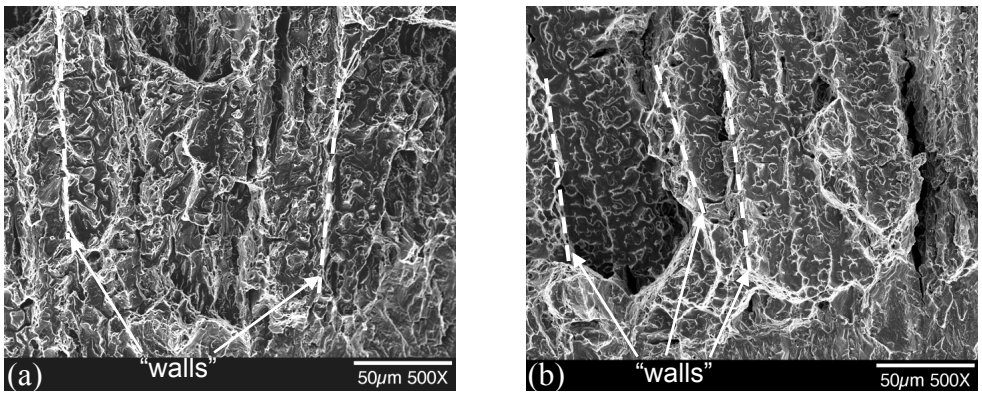

Figure 3: Secondary electron images of fracture surfaces for (a) 21-6-9 and (b) 22-13-5 GTA welds. Crack growth is from bottom to top. Fatigue precracks are at the bottom of images.

that microcracks formed along the weld dendritic structure link up by shear. Shear events may create the vertical sections of steps in Figure 4(a) as well as the "walls" in Figure 3.

4 DISCUSSION

Hydrogen enhanced the fracture susceptibility of 21-6-9 and 22-13-5 GTA welds. The ratio J_{IH}/J_{IC} was 0.14 for 21-6-9 and 0.29 for 22-13-5 welds. In addition to degrading fracture toughness, hydrogen altered the fracture mode in GTA welds. The fracture mode transitioned from predominantly microvoid fracture in uncharged welds to fracture governed by the dendritic microstructure in hydrogen-charged welds.

Based on microscopy evidence, the following physical model is proposed for hydrogen-assisted fracture in 21-6-9 and 22-13-5 GTA welds. Hydrogen promotes the formation of microcracks in δ-ferrite and σ as well as at γ/δ-ferrite and γ/σ interfaces ahead of the fatigue precrack tip (Balch [4]). The oriented weld dendritic structure causes formation of microcracks on parallel planes ahead of the precrack tip. Hydrogen plays an additional role by facilitating localized deformation in the ligament between parallel microcracks. The localized deformation leads to fracture of the ligament and the linking up of microcracks that form along the dendritic structure. These two stages of the fracture process, i.e., microcrack formation along the dendritic structure and microcrack link-up through localized deformation, are reflected in the "stepped" fracture profile of Figure 4(a). The proposed mechanism for fracture in the ligament between microcracks is nucleation of voids at small particles (e.g., MnS) in the band of intense deformation.

The notion that hydrogen could facilitate localized deformation in the ligament between microcracks was tested through a continuum finite-element model (FEM). The material parameters used in the calculations were determined from experiments on a much simpler stainless steel microstructure, i.e., a 21-6-9 forging containing oriented σ-phase stringers. After thermally charging the 21-6-9 forging to a similar hydrogen concentration as the 21-6-9 GTA weld, the forging exhibited hydrogen-assisted fracture and a "stepped" fracture profile, e.g., similar to Figure 4(a).

The FEM solution and determination of hydrogen concentration followed the methodologies described by Liang [5]. The domain used for the boundary value solution was based on the physical model described above, i.e., two microcracks that overlapped on parallel planes were loaded in remote plane-strain tension. In agreement with microscopic studies of the effect of hydrogen on enhancing dislocation mobility [8], the flow stress of the material was assumed to be a decreasing function of the hydrogen concentration. The flow stress used for both hydrogen-

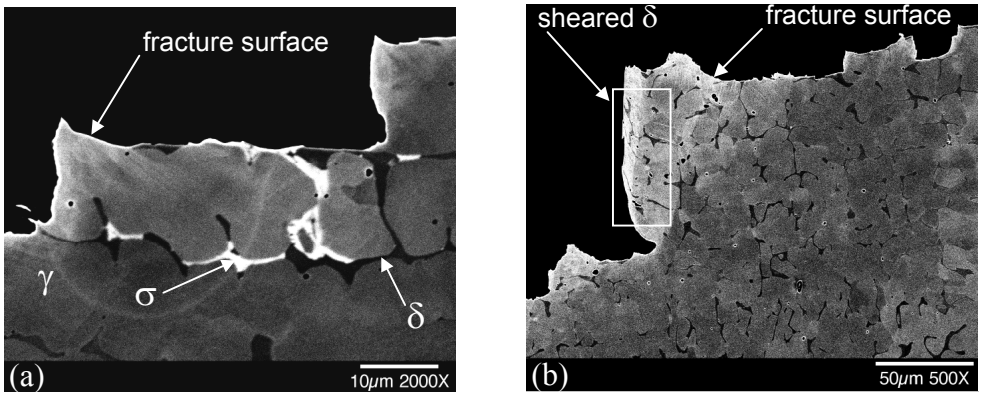

Figure 4: Backscattered electron images of fracture profiles for 22-13-5 GTA welds. Crack growth is parallel to the image (right to left) in (a) and normal to the image (into page) in (b).

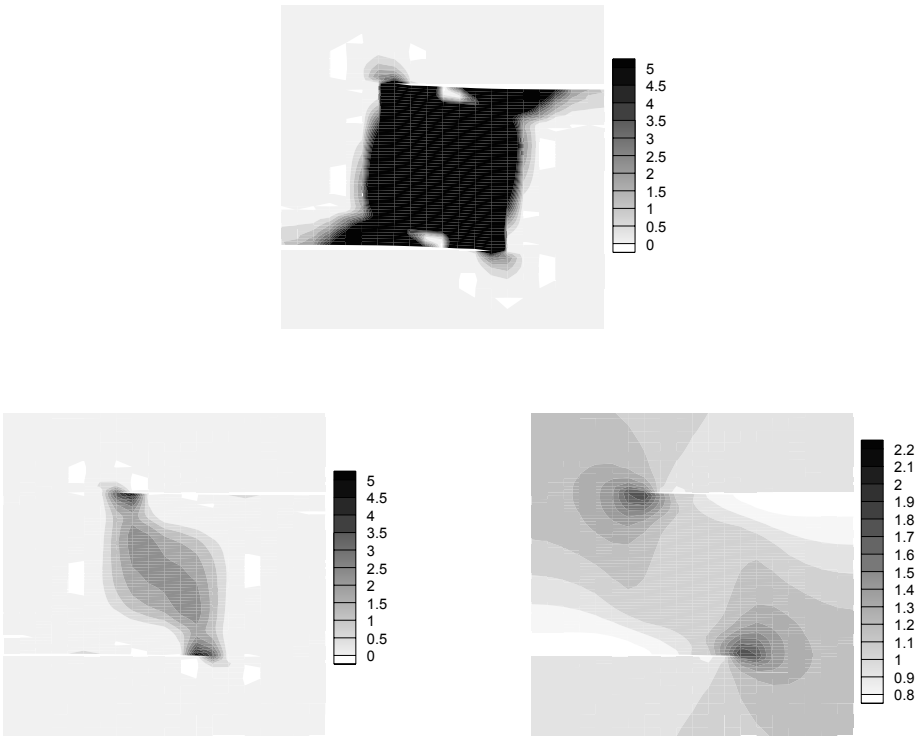

Figure 5: (a) $\varepsilon^p/\varepsilon_0$ distribution for uncharged case (c_0=0) at an applied macroscopic true strain of 0.00336. (b) $\varepsilon^p/\varepsilon_0$ distribution for hydrogen-charged case (c_0=0.015) at an applied true strain of 0.00334. (c) c/c_0 distribution for hydrogen-charged case at an applied true strain of 0.00334.

charged and uncharged materials was $\sigma_Y = \sigma_0[c(\xi-1)+1](1+\varepsilon^p/\varepsilon_0)^N$, where c is the local hydrogen concentration, ε^p is the logarithmic strain, ε_0 and σ_0 are respectively the yield strain and yield stress in the absence of hydrogen, and *N* is the hardening exponent. The parameter ξ was adjusted so that the yield stress of the material (ε^p=0) is reduced to 0.9 σ_0 when c equals the initial hydrogen concentration c_0=0.015 H atoms/solvent atom. The constitutive response of the hydrogen-charged and hydrogen-free material was assumed rate independent with von Mises yielding and associated flow rule. Hydrogen was assumed to reside either at normal interstitial lattice sites or at dislocations generated by plastic flow, which serve as reversible trap sites. The two populations were always in equilibrium according to Oriani's theory (Oriani [6]). The lattice hydrogen concentration was established under equilibrium conditions with the local hydrostatic stress, σ_{kk} (Hirth [7]). No transient effects were considered in the development of the hydrogen concentration, i.e., the hydrogen concentration is known at a point once the effective plastic strain, ε^p, and the hydrostatic stress, σ_{kk}, are known. Due to coupling, the magnitudes of ε^p and σ_{kk} are also dependent on hydrogen. Upon straining, the hydrogen concentration varies pointwise as dictated by local hydrostatic stress and plastic strain and as a result, the material flow characteristics vary pointwise according to the formula above.

The FEM results showed that hydrogen facilitated localized deformation in the ligament between microcracks. Figure 5 shows calculated distributions of the normalized effective plastic strain, $\varepsilon^p/\varepsilon_0$, and normalized hydrogen concentration, c/c_0, around the two parallel, overlapping microcracks. Deformation is very diffuse in the ligament between microcracks for the simulation without hydrogen (Figure 5(a)). In contrast, deformation is localized in a narrow band for the simulation with hydrogen (Figure 5(b)). The development of localized deformation is connected to the redistribution of hydrogen near the tips of microcracks (Figure 5(c)). In fact, it is the inhomogeneity of the local hydrogen distribution responsible for the inhomogeneity in the local flow stress reduction that promotes the localization of deformation into a band of intense shear. Previous FEM simulations showed that small, local perturbations in the initial uniform hydrogen distribution can promote deformation instability (Liang [5]). The results in Figures 5(b) and 5(c) support the notion that hydrogen could have facilitated localized deformation between microcracks in welds, which led to link-up of the microcracks.

5 CONCLUSIONS

- Hydrogen degraded the fracture toughness of 21Cr-6Ni-9Mn GTA welds (J_{IH}/J_{IC}=0.14) and 22Cr-13Ni-5Mn GTA welds (J_{IH}/J_{IC}=0.29).
- Microscopy results suggested that hydrogen served two roles in the fracture of welds: hydrogen promoted the nucleation of microcracks along the dendritic structure, and hydrogen accelerated the link-up of microcracks by facilitating localized deformation.
- A continuum finite-element model supported the notion that deformation could localize in a narrow band between two parallel, overlapping microcracks when hydrogen was assumed to decrease the flow stress at the microscale.

ACKNOWLEDGMENTS

The authors gratefully acknowledge support from the U.S. Dept. of Energy (contract # DE-AC04-94AL85000) and the National Science Foundation (contract # DMR 0302470).

REFERENCES

1. Caskey, G.R., Hydrogen Effects in Stainless Steel, in Hydrogen Degradation of Ferrous Alloys, Noyes Publications, Park Ridge, NJ, 822-862, 1985.

2. Brooks, J.A., et al., Effect of Weld Composition and Microstructure on Hydrogen Assisted Fracture of Austenitic Stainless Steels, Metallurgical Transactions A, **14A**, 75-84, 1983.

3. Standard Test Method for J-Integral Characterization of Fracture Toughness, in Annual Book of ASTM Standards, **03.01**, ASTM, West Conshohocken, PA, 968-991, 1997.

4. Balch, D.K., et al., Microstructural Effects on Hydrogen-Assisted Fracture of Austenitic Stainless Steel Welds, in Corrosion 2004, **04561**, NACE International, Houston, TX, 1-12, 2004.

5. Liang, Y., et al., On the Effect of Hydrogen on Plastic Instabilities in Metals, Acta Materialia, **51**, 2717-2730, 2003.

6. Oriani, R.A., The Diffusion and Trapping of Hydrogen in Steel, Acta Metallurgica, **18**, 147-157, 1970.

7. Hirth, J.P. and Carnahan, B., Hydrogen Adsorption at Dislocations and Cracks in Fe, Acta Metallurgica, **26**, 1795-1803, 1978.

8. Birnbaum, H.K. and Sofronis, P., Hydrogen-Enhanced Localized Plasticity - A Mechanism for Hydrogen-Related Fracture, Materials Science and Engineering, **A176**, 191-202, 1994.